



## Tsunami-Sediment Interactions Amplify Coastal Hazard and Reshape Inundation Dynamics in Tumaco Bay, Colombia

Ronald E. Sanchez Escobar<sup>1</sup>, Juan Jose Ferrer<sup>2</sup>, Erick R. Velasco-Reyes<sup>3</sup>, and Erick Mas<sup>4</sup>

Correspondence: Erick Mas (mas@tohoku.ac.jp)

Abstract. Tumaco, situated on the Colombian Pacific coast, is particularly vulnerable due to its location within the Pacific Ring of Fire. Although studies on tsunami risk in the region have been conducted, the interaction between these events and sediment transport has been little explored, despite its impact on flooding dynamics. This study addresses this gap by comparing two scenarios — those with and without sediment transport — and evaluating the morphodynamic effects of tsunami events on proposed mitigation measures for Tumaco. The results show that including sediment transport in the simulations increases wave heights, flooding depth and extent, as well as coastal impacts. In particular, maximum flood depths increase by 24.4% on Morro Island, 11.57% on Tumaco Island, and 30.91% on the mainland. Likewise, flooded areas increase by 4.12%, 5.15%, and 13.43%, respectively, due to increases in flow density and momentum. The mitigation measures reduce the extent of flooding, although they cause local increases in wave heights due to reflection effects. It is noteworthy that in the simulations with mitigation measures, sediment transport does not cause erosion that compromises these coastal defenses. These findings underscore the importance of incorporating sediment transport into tsunami modeling to enhance hazard assessments and refine mitigation strategies, ultimately contributing to the development of more effective coastal resilience plans.

#### 1 Introduction

Tsunamis are natural phenomena containing a large amount of hydrodynamic energy, capable of transporting materials of various types and sizes, from fine particles to large blocks, over distances that can reach several kilometers inland (Sugawara et al., 2014; Masaya et al., 2020). Recent research has shown that the interaction between a tsunami, coastal morphology, and sediment transport can significantly modify the run-up, a critical factor in assessing tsunami hazards (Yamashita et al., 2016; Apotsos et al., 2011; Velasco-Reyes et al., 2024) and evacuation planning (Mas et al., 2015, 2024). The Colombian Pacific coast is particularly exposed to tsunamis due to its intense seismic activity related to the "Pacific Ring of Fire," where subduction processes occur between the South American and Nazca tectonic plates (Gutscher et al., 1999; Collot et al., 2009). Significant seismic events, such as those in 1906 (Mw 8.6) and 1979 (Mw 8.2), have been associated with the generation of devastating

<sup>&</sup>lt;sup>1</sup>Centro de Investigaciones Oceanográficas e Hidrográficas del Pacífico (CCCP), Dirección General Marítima (DIMAR), Tumaco, Colombia

<sup>&</sup>lt;sup>2</sup>Marine and Coastal Geosciences Program, Marine and Coastal Research Institute "José Benito Vives de Andréis" (INVEMAR)

<sup>&</sup>lt;sup>3</sup>Oregon State University, College of Engineering, School of Civil and Construction Engineering, Oregon, US

<sup>&</sup>lt;sup>4</sup>International Research Institute of Disaster Science, Tohoku University, Sendai, Japan





tsunamis, particularly along the Colombian Pacific coast, resulting in tragic consequences for the Tumaco population (Sánchez et al., 2020; Usselmann, 2010). Despite numerous studies conducted to quantify the level of hazard faced by the population of Tumaco (e.g., (Caballero and Ortiz, 2003; Cardona et al., 2005; Sánchez and Puentes, 2012; Guerrero and Sánchez, 2016; Otero and González, 2004; Sánchez et al., 2020), none of these consider the interaction between the tsunami and sediment transport, and its effect on numerical flood modeling. This omission may lead to an inadequate risk estimation, since including this parameter can increase the flow density and tsunami momentum, altering predictions of run-up and flood depth (Cheng and Weiss, 2013; Sugawara et al., 2014). Furthermore, including this factor could induce morphological changes along the coast, related to erosion and sedimentation processes, which in turn could modify the tsunami's behavior and dynamics, affecting its propagation, intensity, and flooding patterns in coastal areas (Shimozono et al., 2012; Jaffe et al., 2016; Apotsos et al., 2011). This study aims to assess the tsunami hazard level in Tumaco by integrating morphodynamic effects and analyzing sediment transport induced by the event. For this purpose, numerical simulations were carried out using the Delft3D model for flood propagation and the D-Morphology module to investigate the impact on morphodynamics and sediment transport in the study area (Deltares, 2023). This approach aims to determine whether including this factor modifies the hazard assessment, particularly regarding run-up and flood depth for the Tumaco population. Additionally, the morphological changes that could occur will be analyzed, and areas susceptible to significant erosion and deposition processes will be identified. Finally, the mitigation alternatives proposed by the Universidad del Norte and the Dirección General Marítima (Dimar) (Universidad del Norte and DIMAR, 2021) will be evaluated to determine whether these solutions provide adequate protection against tsunami events, thereby ensuring the community's safety and establishing a baseline to guide research, actions, resources, and policies to be implemented in the medium and long term for the development of disaster risk reduction programs and sustainable coastal development.

#### 2 Study area

This study focuses on the municipality of Tumaco, situated in the southwest of the Colombian Pacific coast, in the Nariño department. It borders the municipalities of Francisco Pizarro, Roberto Payán, and Mosquera to the north; Barbacoas to the east; the Republic of Ecuador to the south; and the Pacific Ocean to the west (Fig. 1). This region is part of the Pacific Ring of Fire, making it a highly vulnerable area to seismic tsunamis (Otero and González, 2004). According to projections from the National Administrative Department of Statistics (DANE) for 2024, Tumaco has approximately 267,000 inhabitants (DANE, 2018). Moreover, considering the socioeconomic context and the structural conditions of the housing, which include stilt houses (Rivas, 2020), the need to focus efforts on mitigating the effects of a possible tsunami becomes evident.





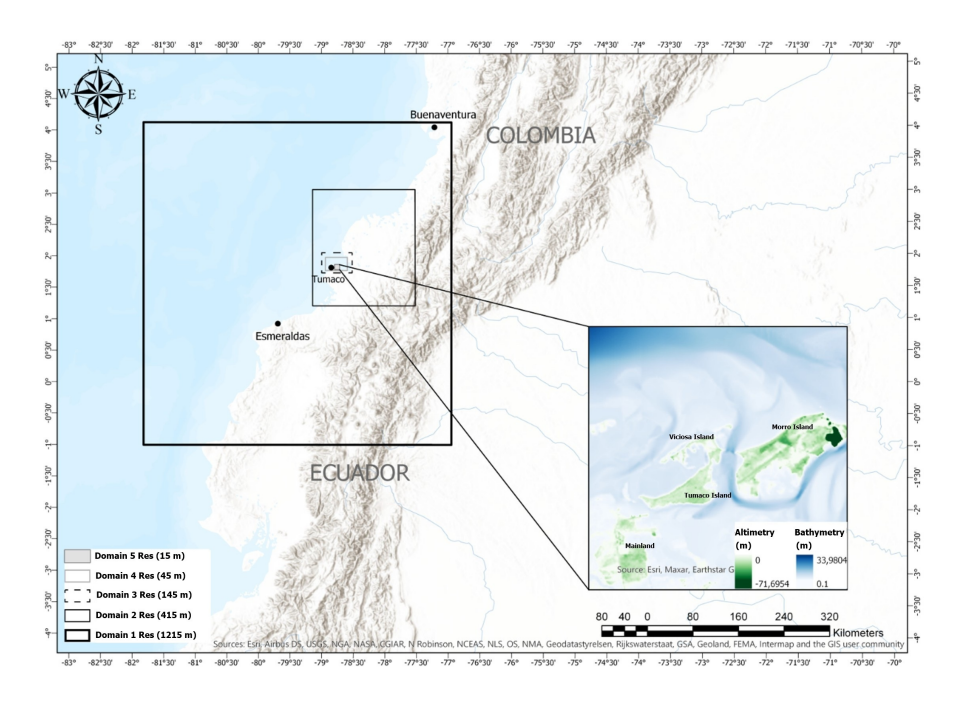


**Figure 1.** Map of the study area and computational domains. Elaborated by the authors, the background basemap corresponds to ESRI Topography in ArcGIS Pro (version 3.0.1).

#### 50 3 Methodology

#### 3.1 Seismic Scenarios (Source Model)

The scenario considered for evaluation corresponds to the worst-case scenario for the Colombian-Ecuadorian subduction zone, proposed by (Poveda and Pulido, 2019) using the slip deficit model. This model is based on the accumulation of interseismic slip deficits along the subduction zone, which represent the tectonic deformation accumulated between significant seismic events. Specifically, the worst-case scenario is defined as the combination of slip deficits considering the 1906 and 1979 earth-quakes, with an estimated magnitude between Mw 8.8 and 8.9, implying a simultaneous rupture of the northern segments of Esmeraldas, Manglares, and Tumaco. Although this scenario is hypothetical and aims to define the largest possible megathrust along the Colombian-Ecuadorian subduction margin, there are no historical records suggesting that an event of such magnitude has occurred in the region (Sánchez et al., 2020). This scenario is modeled using 969 subfaults, each with an area of  $10 \times 10$  km, a strike of  $30^{\circ}$ , a dip of  $15^{\circ}$ , and an azimuth angle of  $118^{\circ}$ . Each event occurs along the Ecuador-Colombia subduction zone (Poveda and Pulido, 2019). The tsunami generation phase, i.e., the seabed deformation, is calculated using the elastic deformation model proposed by (Okada, 1992). This model assumes an instantaneous static deformation of the sea surface, which is identical to the vertical displacement of the seafloor (Sánchez et al., 2013).





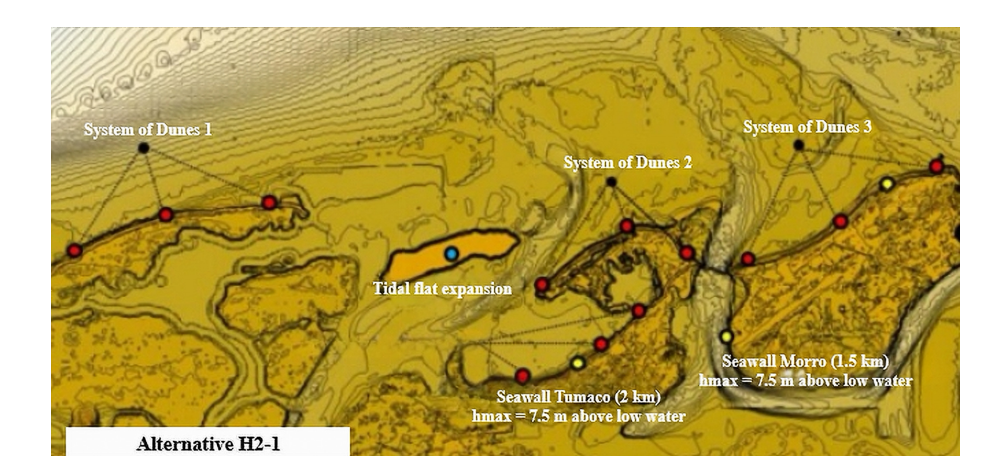


**Figure 2.** Map including the evaluated mitigation measures. Elaborated by the authors.

#### 3.2 Numerical Modeling

The simulation of tsunami propagation and inundation was carried out using the Delft3D model, which allows for the simulation of hydrodynamic processes occurring during tsunami propagation and coastal flooding (Deltares, 2023; Watanabe et al., 2018). Delft3D solves the nonlinear shallow water equations (NLSWEs) using a finite-difference scheme (Stelling and van Kester, 1994), where the conservation of mass and momentum governs wave propagation. Several studies have validated this model, producing optimal and reliable results (Linlin and Zhenzhua, 2013; Jaffe et al., 2016; Watanabe et al., 2018). For the modeling, five nested computational domains were defined (Table 1). The outermost domain (1) covers the precursor earthquake generation zone, while the subsequent domains (2, 3, and 4) represent the propagation of tsunami waves from deep to shallow waters. Finally, the inundation phase is analyzed in the innermost domain (5). For domains 1, 2, and 3, bathymetric data from the General Bathymetric Chart of the Oceans (GEBCO) were used. In contrast, for the higher spatial resolution domains (4 and 5), altimetric and bathymetric information provided by the Centro de Investigaciones Oceanográficas e Hidrográficas del Pacífico (CCCP), according to the standards of the National Hydrographic Service, was employed, supplemented with data obtained from field campaigns in the study areas (Table 1). It is essential to highlight that the inundation phase was evaluated in two different contexts, using two configurations of domain 5 (Fig. 1). In the first case, the current situation of the population without interventions was simulated. In the second, the mitigation works proposed in the project Studies for the implementation of actions to mitigate the effects of tsunami and climate change hazards in the municipalities of Tumaco and Francisco Pizarro (Universidad del Norte and DIMAR, 2021) were incorporated, allowing for a comparison between both contexts. The evaluated alternative was H2-1, which includes four dune systems, the expansion of a tidal flat, and two seawalls

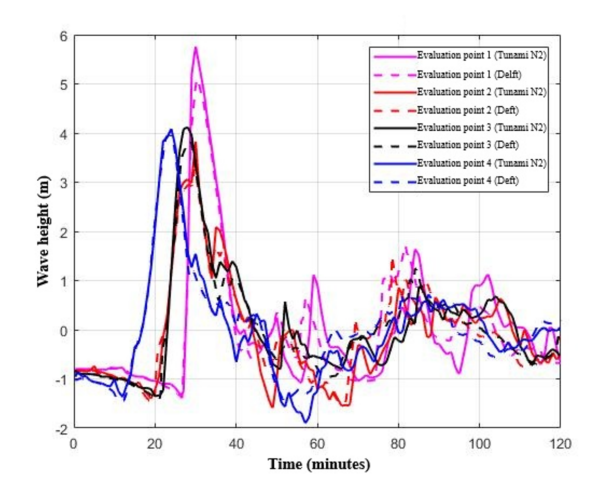
The Delft3D model enables the incorporation of advective terms, allowing for the calculation of unsteady flow, sediment transport, and morphological changes, while integrating parameters such as roughness, initial sediment thickness, grain size, and density (Deltares, 2023; Velasco-Reyes et al., 2024). Sediment transport is determined through the D-Morphology module





Table 1. Configuration of the computational domains

Domain	Low Left boundary	Upper right boundary	Number of cells in x	Number of cells in y	Resolution (m)
5	-78,80; 1,78	-78,72; 1,86	592	607	15
4	-78,94; 1,76	-78,60; 1,97	856	514	45
3	-79,00; 1,72	-78,52; 2,04	397	262	135
2	-79,14; 1,20	-77,52; 3,04	445	505	405
1	-81,80; -1,00	-76,94; 4,11	445	467	1215



**Figure 3.** Synthetic tide gauge. Solid lines: results obtained using the TUNAMI N2 model. Dashed lines: results obtained using the Delft3D model.

by solving the mass conservation equations within the hydrodynamic model, based on the equations proposed by van Rijn (2007) for suspended sediment transport and bed load transport (Deltares, 2023). Research conducted by (Lesser et al., 2004; van Rijn, 2007) has demonstrated that Delft3D adequately models sediment transport and morphological changes. To validate the model results for the population of Tumaco, a comparison was made between the model to be used (Delft3D) and the Tsunami N2 model, since the latter has already been validated for this population and has been employed in studies such as Sánchez et al. (2020); Adriano et al. (2025); Guerrero and Sánchez (2016), among others. Validation was carried out by comparing a synthetic tide gauge at several evaluation points, located at the exact coordinates for both models. The coordinates of the evaluated points are presented in Table 2, and the results of the synthetic tide gauge are shown in Fig. 3. From this comparison, a high correlation was determined with an average Pearson coefficient of 0.96 for the evaluation points, thus providing a proper validation of the Delft3D model for this study area.





Table 2. Evaluation points

Evaluation points	Coordinates		
	Latitude	Longitude	
1	1,825	-78,773	
2	1,824	-78,746	
3	1,838	-78,761	
4	1,852	-78,793	

#### 3.3 Parameters Used in the Simulation and Sensitivity Analysis

For the simulation, a uniform Manning coefficient of 0.02 was applied in both the u and v directions. The horizontal turbulent viscosity (eddy viscosity) and horizontal turbulent diffusivity (eddy diffusivity) were set to 0.1. The time step was 0.01 minutes, with a total simulation duration of 3 hours. Regarding the boundary conditions, a high tide was used as the tidal condition, with a tidal range of 3.6 meters, corresponding to the 95th percentile of the total tidal range recorded in the study area. Studies such as those by Takahashi et al. (2011); Velasco-Reyes et al. (2024) have demonstrated the crucial role of grain size in the transport of non-cohesive sediments during tsunamis. In this context, it is essential to consider a variety of grain sizes when modeling to assess their variability and estimate the uncertainty range associated with this input parameter. For this purpose, a sensitivity analysis of the average sediment thickness was conducted as a function of grain size, using the same seismic conditions with five different sizes: 80, 110, 140, 170, and 200 µm (Fig. 4b). The selection of these sizes was based on results obtained by measuring sediment size in the water column using the LIST instrument (Fig. 4a) at a specific point with coordinates 1.84° N, 78.73° W. Next, the thickness distribution was calculated for each of the five grain sizes. An envelope distribution was established, normalized using the grain size of 140  $\mu$ m as the reference value (Fig. 4c). The results ranged from 0.7 to 1.3, with a mean of 1.03, generating an uncertainty range of  $\pm 0.3$ , which covers the minimum to the maximum grain size evaluated. Similarly, a sensitivity analysis was carried out regarding the initial sediment availability. Simulations were performed with different initial sediment thicknesses, maintaining a constant grain size of 140 µm (Fig. 5). The thicknesses evaluated were 2, 3, 4, 5, and 6 m. Subsequently, an envelope distribution was established to represent the uncertainty margin associated with sediment availability, taking a 4 m thickness as the reference parameter. The results were extracted from a uniform distribution ranging from 0.97 to 1.04, with a mean of 1.005, resulting in an uncertainty range of  $\pm 0.035$ .

#### 115 4 Results and Discussion

#### 4.1 Effect of Sediment Transport on Wave Propagation and Flood Dynamics in the Current State

Figure 6, divided into three sections, shows the maximum tsunami height for the two simulation conditions (sections a and b). In contrast, section c displays the difference between the two heights. Likewise, Table 3 details the maximum height,



125



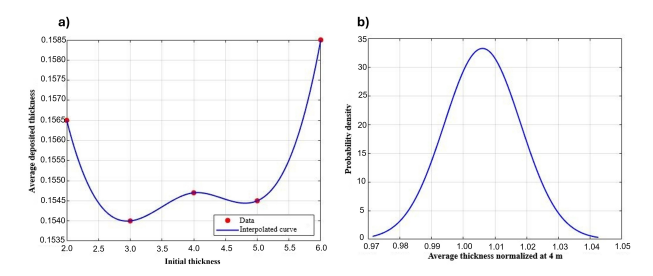


Figure 4. a) Average sediment thickness as a function of initial thickness with a grain size of 140  $\mu$ m. b) Normalized envelope distribution relative to the initial thickness of 4 m

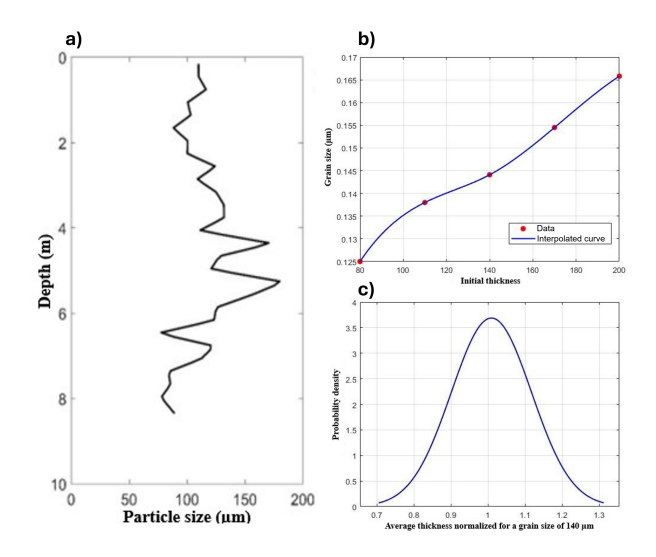


Figure 5. a) Sediment size was measured using the LIST instrument in the study area. b) Average sediment thickness as a function of grain size. c) Normalized envelope distribution relative to the grain size of  $140 \mu m$ .

maximum inundation distance, maximum inundation depth, and inundation area for the two simulation conditions and the two evaluated contexts. In the condition without considering sediment transport (Fig. 6a), wave heights range from 2 to 5.6 m in the shallow waters of the study area, with their maximum values occurring near Morro Island (Table 3). For Tumaco Island and the mainland, the heights are 5 m and 2.92 m, respectively. Sánchez et al. (2020) report a similar wave distribution in this scenario, although with a maximum value of 4.66 m, lower than that recorded in this study. This difference could be attributed to bathymetric changes, since the data used in this study are more recent and reflect the constant changes in the seabed of Tumaco Bay (Cantero et al., 2023). On the other hand, in the simulation including sediment transport (Fig. 6b), wave heights are greater, ranging from 2.20 to 6.60 m. In this case, wave heights reach 6.60 m, 5.30 m, and 3.78 m near Morro Island, Tumaco Island, and the mainland, respectively. This difference is clearly illustrated in Fig. 6c, which shows the difference between the conditions with and without sediment transport. In this section, positive values, represented by yellowish and reddish tones,



130

135

140

145

150

155

160



indicate higher wave heights in the simulation with sediment transport, with an average difference of 0.26 m and positive differences reaching up to 2.20 m in areas such as Bajito on Tumaco Island, where various houses and tourist establishments are located. To analyze the tsunami behavior in both scenarios in more detail, a synthetic tide gauge (Fig. 7) was created at two points near the coasts of Morro and Tumaco Islands (Points 1 and 2, Table 2). During the first 25 minutes, both simulations exhibit similar behavior, characterized by an initial retreat of water. From this moment, with the arrival of the first tsunami wave, corresponding to the maximum peak height, differences begin to appear between the two simulation conditions, being greater in the one that incorporates sediment transport. At Point 1, the maximum height is recorded at minute 30, reaching 5.93 m in the simulation with sediment transport, which represents an increase of 0.21 m compared to the simulation without this factor. At Point 2, the first wave arrives two minutes earlier, recording a maximum value of 4.26 m, 0.17 m higher than in the simulation without sediment transport. After the impact of the first wave, differences between the two simulations persist throughout the record. At Point 1, after the maximum peak at minute 30, wave heights in the simulation with sediment transport remain between 0.10 m and 0.55 m above the simulation without sediment transport for the following 40 minutes. At Point 2, this difference is minor, with values ranging from 0.08 m to 0.39 m. Likewise, Figure 8 shows both the extent and depth of inundation for the two previously mentioned conditions (sections a and b), as well as the difference in these parameters (section c). From this figure, it is observed that the condition with sediment transport presents a greater extent of inundation, reaching maximum values of 1.38 km on Morro Island, 0.91 km on Tumaco Island, and 0.77 km on the mainland. In comparison, under the condition without sediment transport, inundation extends up to 1.34 km, 0.7 km, and 0.63 km in the same sectors. This is also reflected in the greater extent of inundation areas under the sediment transport condition (Table 3), which are 4.12%, 5.15%, and 13.43% larger in the sectors of Morro Island, Tumaco Island, and the mainland, respectively. The condition with sediment transport also shows greater inundation depths, with maximum values of 6.22 m on Morro Island, 4.81 m on Tumaco Island, and 3.43 m on the mainland (Fig. 8b), representing an increase of 24.4%, 11.57%, and 30.91%, respectively, compared to the condition without sediment transport (Fig. 8a) (Table 3). This increase is evident in Figure 8c), where positive values predominate in most sectors, with differences of up to 1.42 m, 1.26 m, and 1.18 m in the aforementioned sectors. Likewise, Table 4 shows a comparison of inundation depths at specific points of interest in the population under conditions with and without sediment transport.

To detail the changes in inundation extent more precisely between the two simulation conditions, the inundation extent at minutes 30, 32, and 34 after the tsunami origin is presented (Fig. 9). It is observed that at all evaluated time points, the condition with sediment transport shows a greater extent. At minute 30, differences reach up to 0.11 km, 0.14 km, and 0.16 km for Morro Island, Tumaco Island, and the mainland, respectively. At minute 32, differences increase to 0.17 km, 0.38 km, and 0.22 km in these same sectors, while at minute 34, differences are 0.13 km, 0.24 km, and 0.18 km. In this latter case, for Tumaco Island, the condition with sediment transport already shows complete inundation in that sector. Similar results were reported by Yamashita et al. (2016) in Hirota Bay, where they compared inundation areas and heights along a profile at different times. Their simulations showed that including sediment transport generates higher values in these parameters compared to scenarios without transport, demonstrating the impact of this factor on water level rise processes. The observed differences in wave height, inundation extent, and inundation depth between the two evaluated conditions can be attributed to both an increase in





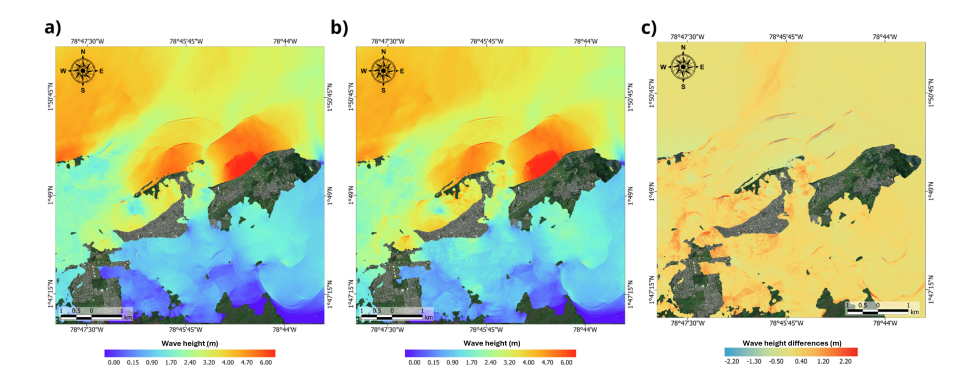


**Figure 6.** Maximum tsunami height under the non-intervention scenario. Condition: a) no sediment transport, b) with sediment transport, c) height differences. Elaborated by the authors, the background basemap corresponds to ESRI Satellite Imagery in ArcGIS Pro (version 3.0.1).

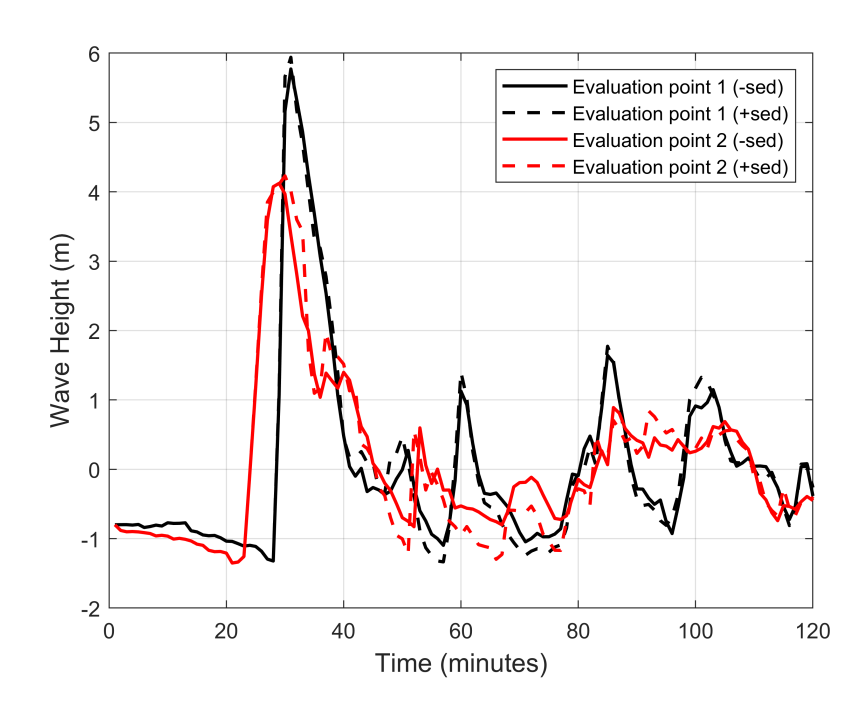


Figure 7. Synthetic mareogram. Solid lines: without sediment transport. Dashed lines: with sediment transport.

flow density, mass, and resulting momentum, as well as to morphological changes induced by the incorporation of sediments.

Xiao et al. (2010) argue that the addition of sediments modifies flow conditions by increasing their density due to the higher mass. This increase favors greater energy conservation during tsunami propagation, resulting in a more energetic flow. Although sediment-induced friction can slightly reduce velocity, the effect is compensated by the additional mass, facilitating greater energy transfer toward the coast. (Apotsos et al., 2011) demonstrates this behavior by showing that flows with high sediment



180



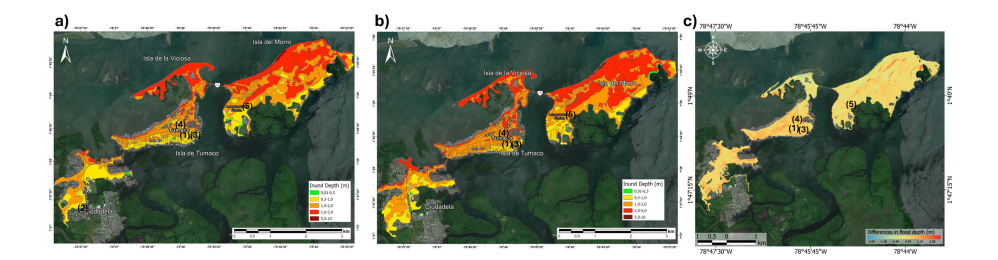


**Figure 8.** Maximum tsunami depth. Condition: a) without sediment transport, b) with sediment transport, c) depth differences. Elaborated by the authors, the background basemap corresponds to ESRI Satellite Imagery in ArcGIS Pro (version 3.0.1).

Table 3. Hydrodynamic and Tsunami Inundation Parameters

Sector	Contexts	Conditions	Maximum tsunami height (m)	Maximum inundation extent (km)	Maximum inundation depths (m)	Inundation area (km <sup>2</sup> )
Morro Island	Without Intervention	Without sediment transport	5.60	1.34	5.00	3.88
		With sediment transport	6.61 (+18.03%)	1.38 (+2.98%)	6.22 (+24.4%)	4.04 (+4.12%)
	With mitigation measures	Without sediment transport	6.86	0.49	4.00	0.87
		With sediment transport	7.63 (+11.22%)	0.54 (+10.20%)	5.55 (+38.75%)	1.09 (+25.28%)
Tumaco Island	Without Intervention	Without sediment transport	5.00	0.70	4.32	1.94
		With sediment transport	5.3 (+6%)	0.91 (+30%)	4.81 (+11.57%)	2.04 (+5.15%)
	With mitigation measures	Without sediment transport	5.56	0.67	3.02	1.29
	magaron measures	With sediment transport	5.8 (+4.31%)	0.78 (+16.41%)	3.52(+16.55%)	1.52(+4.12%)
Continent	Without Intervention	Without sediment transport	2.92	0.63	2.62	1.34
		With sediment transport	3.78 (+29.45%)	0.77 (+22.22%)	3.43(+30.91%)	1.52 (+13.43%)
	Con medidas de mitigación	Sin transporte	3.12	0.48	2.22	1.26
	Con medical de integación	Con transporte	3.25 (7.37%)	0.62 (+29.16%)	2.76(+24.32%)	1.42 (+12.69%)

concentrations alter velocity and transport structures, conserving more energy near the shore. Consequently, a greater run-up and a larger inundation extent are observed. Moreover, associated morphodynamic processes, such as erosion and deposition, modify the wave–coast interaction, intensifying the magnitude of run-up and inundation depth (Masaya et al., 2020).

# 4.2 Effect of Sediment Transport on Wave Propagation and Inundation Dynamics in the Context of Mitigation Measures

Figure 10 illustrates the maximum tsunami height under two simulation conditions, considering the context of mitigation measures. In this scenario, higher wave heights are observed compared to the no-intervention context, except on the mainland sector, where no mitigation measures were implemented. In the simulation without sediment transport, recorded wave heights were 6.86 m, 5.56 m, and 3.12 m for Morro Island, Tumaco Island, and the mainland, respectively (Fig. 10a). This increase in wave height compared to the no-intervention context is attributed to the reflection generated by the dunes and seawalls. These structures not only cause part of the wave to return to the ocean but also concentrate its energy near the coast. The reflected wave interacts with the incoming wave, resulting in an increase in wave height due to constructive interference. Ning et al. (2017)



190

195



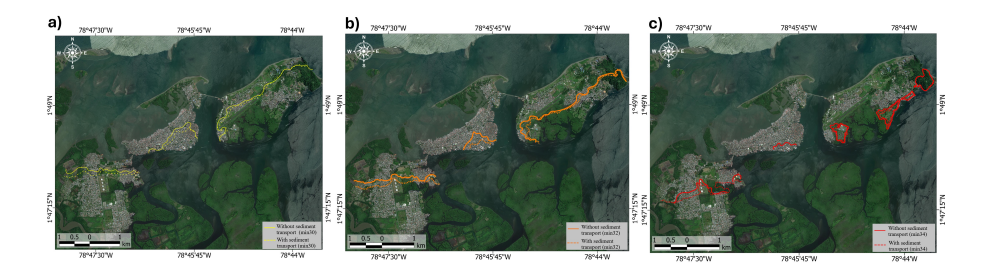


**Figure 9.** Comparison of the inundation extent at minutes 30 (a), 32 (b), and 34 (c). Solid lines: without sediment transport. Dashed lines: with sediment transport. Elaborated by the authors, the background basemap corresponds to ESRI Satellite Imagery in ArcGIS Pro (version 3.0.1).

Table 4. Variation of inundation depths with and without sediment transport at points of interest

Points of Interest	Inundation Depth (m)		
	Without sediment transport	With sediment transport	
City Hall (1)	0.89	1.41	
Divino niño Hospital (2)	0	0.38	
Fire Department (3)	0.79	1.19	
Police Command (4)	0.65	0.97	
Airport (6)	0.91	1.18	

observed that this phenomenon can raise free surface elevation to 2.6 times due to the interaction between incident and reflected waves. In the scenario with sediment transport, higher wave heights are also observed, reaching 7.63 m, 5.8 m, and 3.25 m on Morro Island, Tumaco Island, and the mainland, respectively (Fig. 10b). This trend is reflected in (Fig. 10c), which shows positive values in most sectors. Although wave heights are greater in the context of mitigation measures, the inundation extent and depth are significantly lower. This is because the impact of the higher waves is concentrated in the areas where dunes and seawalls are located. However, as the ground elevations increase due to the implementation of these structures, the inundation depth and extent are reduced. In the simulation without sediment transport, inundation penetration is reduced to 0.49 km, 0.67 km, and 0.48 km in the sectors of Morro Island, Tumaco Island, and the mainland, respectively, representing decreases of 63.44%, 4.28%, and 23.80% in these sectors. This reduction is also reflected in the decline in inundated areas, with reductions of 77.57%, 33.50%, and 5.98% in the corresponding regions (Table 3). In the scenario with sediment transport, inundation penetration also decreases to 0.54 km, 0.72 km, and 0.54 km for the same sectors, representing reductions of 60.87%, 21.88%, and 29.88%, respectively. This change is also reflected in the decrease in inundated areas in these sectors. Regarding inundation depths, both scenarios with mitigation measures show lower values compared to the no-intervention context, with differences ranging from 0 to 3.4 m (Figs. 8 and 11). Maximum differences are recorded in the beach zones of Morro Island and El Bajito on Tumaco Island, where mitigation works have been proposed. However, within these scenarios, the simulation including





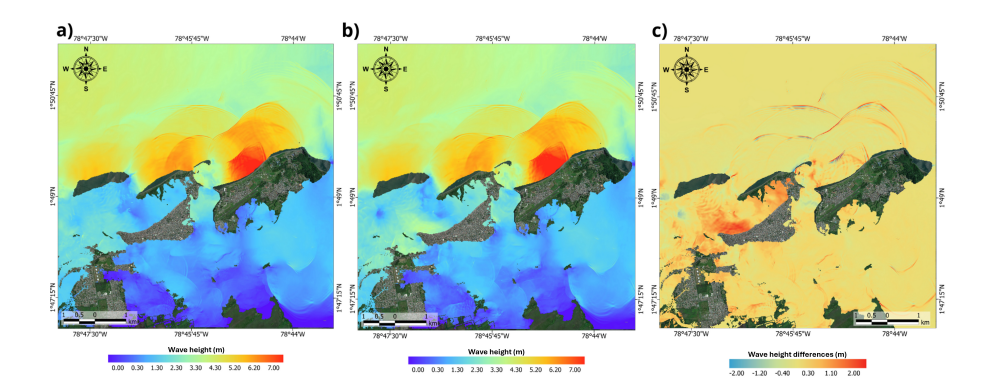


**Figure 10.** Maximum tsunami height for the mitigation scenario. Condition: a) without sediment transport, b) with sediment transport, c) height differences. Elaborated by the authors, the background basemap corresponds to ESRI Satellite Imagery in ArcGIS Pro (version 3.0.1).

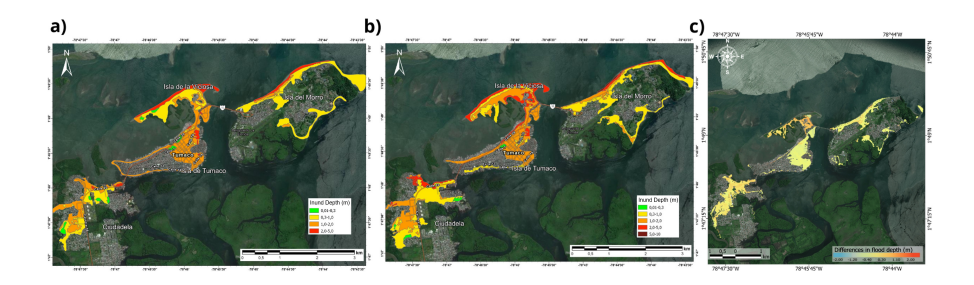


**Figure 11.** Maximum tsunami depth for the mitigation scenario. Condition: a) without sediment transport, b) with sediment transport, c) depth differences. Elaborated by the authors, the background basemap corresponds to ESRI Satellite Imagery in ArcGIS Pro (version 3.0.1).

sediment transport presents greater inundation depths (Figs. 11a and 11b). This is evidenced by the predominance of positive values in the inundation depth differences (Fig. 11c), with an average of 0.28 m and maxima of 1.4 m, 0.9 m, and 0.86 m in the zones of Morro Island, Tumaco Island, and the mainland, respectively (Table 3). Taken together, these results, along with the reduction in inundation extent and area, indicate that the mitigation measures proposed by Universidad del Norte and DIMAR (2021) contribute significantly to reducing the tsunami hazard level in the study area.

### 4.3 Resulting Morphological Changes

200

205

Figure 12 illustrates the morphological changes that occurred following the tsunami in the two analyzed inundation contexts. In this figure, negative values represent areas affected by erosion, while positive values correspond to zones where sediment accumulation has occurred. In the no-intervention context (Fig. 12a), representing the current situation, marked erosion is identified on Morro Island, particularly along the coastal strip exposed to the tsunami impact, with values up to 2.4 m in the northern and northeastern sectors, where the beach is located. Likewise, the western part of the island, near the bridge connecting it to Tumaco Island, shows the highest erosion values, reaching up to 2.8 m. In contrast, in the southern and



210

215

220

225

230

235

240



southeastern parts, areas of sediment deposition are evident, suggesting that the inundation flow transported sediment and redistributed it in lower-energy zones. The interaction between the island's topography and its orientation appears to have influenced sediment dynamics, resulting in sectors with differential sediment accumulation. For Tumaco Island, significant erosion is recorded in the frontal area, which receives the direct impact of the tsunami. This zone, known as El Bajito, features a strip approximately 400 meters long, with erosion values reaching up to 3.74 m, indicating intense sediment removal due to the combined action of the incoming flow and the return current. In contrast, in more sheltered and internal sectors, such as the rear part of El Bajito, sediment deposition of up to 2.45 m is recorded, suggesting a lower-energy environment where suspended materials were able to settle. The sediments eroded from the frontal strip would have been transported and deposited in this lagoon area, favoring their accumulation in calmer waters. On the mainland, located at the lower left side of the map, the morphological changes are less pronounced. Some areas with moderate erosion are identified, with values close to -1.20 m, particularly near water bodies and natural channels, indicating that the tsunami flow caused some sediment to be dragged in these sectors. Small areas of deposition are also recorded, possibly associated with the loss of flow energy in zones with a lower slope or more protected areas. In general, this can be attributed to the direction of the tsunami, which impacted the islands more strongly before reaching the mainland, dissipating part of its energy. Additionally, this area is protected by Boca Grande, a natural barrier that may have reduced the intensity of the incoming flow. The combination of these factors, along with the topography, contributed to less sediment redistribution in this area. Figure 11b illustrates the morphological changes resulting from the interventions. In general, the application of mitigation measures has reduced erosive and depositional processes on the emerged land. When compared to the no-intervention scenario, morphological changes are practically negligible in large areas, especially on the islands and the mainland. On Morro Island, erosion reduction is evident in the beach sector, reaching up to 2.28 m, as well as a lower sediment deposition in areas farther from the shoreline. For Tumaco Island, considerable erosion is no longer observed in the El Bajito area, achieving a reduction of up to 3.48 m. In this context, the area with the most significant erosion is located on the sides of the tidal flat, which acts as a mitigation measure by protecting both Tumaco Island and the mainland. In this zone, erosive processes reach up to 3.11 m, and the removed sediments are transported and deposited immediately behind the tidal flat, where an accumulation of up to 1.90 m is recorded. The presence of a sediment plume in this area suggests that the tidal flat favors the dissipation of flow energy and the deposition of transported material, thus contributing to the stabilization of the coastal environment. Finally, on the mainland, no significant morphological changes are evident, similar to the scenario without interventions. This indicates that the mitigation measures are not only effective in reducing the threat in terms of inundation depth, extent, and area but also contribute to relief stability by minimizing erosion and sediment redistribution. Their capacity to dissipate flow energy suggests that these strategies can maintain their effectiveness over time and serve as lasting protection against future tsunami events.

#### 5 Conclusions

This study evaluated tsunami hazard in four scenarios under two conditions: with and without sediment transport, as well as in two mitigation contexts: without intervention (current situation) and with intervention. The results demonstrate that the in-



250

255



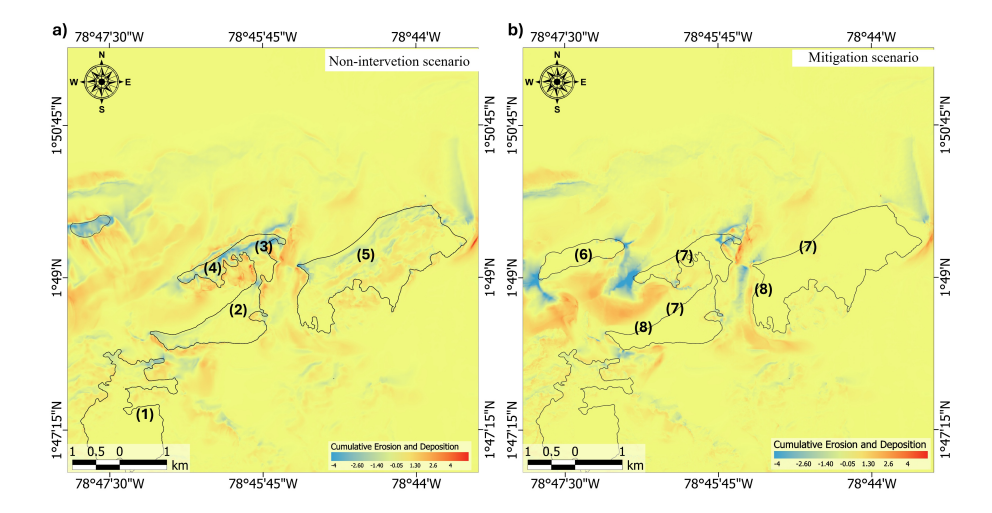


Figure 12. Distribution of tsunami accumulation, erosion, and deposition. a) Non-intervention scenario, b) Mitigation scenario. Negative values indicate erosion, while positive values indicate deposition. Zones: (1) Mainland. (2) Tumaco island. (3) El Bajito. (4) Viciosa Island. (5) Morro Island. (6) Tidal flat expansión. (7) Dune System. (8) Seawall.

clusion of sediment transport in tsunami modeling is a crucial factor in coastal hazard assessment, as the interaction between tsunami flow and sedimentary dynamics significantly alters inundation patterns, thereby intensifying the hazard level. In particular, there is an observed increase in the rate of water rise and in inundation depth, with the latter variable showing increases of 24.4% on Isla del Morro, 11.57% on Isla de Tumaco, and 30.91% on the mainland. Likewise, inundation extent increases by 2.98%, 30%, and 22.22%, and this effect is also reflected in the affected area, which expands by 4.12%, 5.15%, and 13.43%, respectively, compared to the simulation without sediment transport. Furthermore, incorporating this process enables the estimation of morphological changes that may occur during a tsunami, providing relevant information for risk management and the development of more accurate mitigation strategies, particularly in the practical design of mitigation measures. The comparison between scenarios without intervention and those with mitigation alternatives demonstrates that the implementation of appropriate strategies not only significantly reduces the extent and depth of flooding but also contributes to the stability of the sedimentary environment. In the non-intervention scenario, erosional and depositional effects result in drastic changes to coastal morphology, thereby increasing the vulnerability of exposed communities. In contrast, in the mitigation scenario, a significant reduction in erosion is observed in critical areas, along with a more controlled redistribution of sediments, which favors the preservation of coastal landforms and ensures long-term morphological stability. This suggests that such strategies are not only effective in reducing hazards in individual events but can also be sustainable and replicable, addressing multiple future events and providing a resilient solution for coastal risk management. The results of this study underscore the importance of incorporating sediment transport into tsunami modeling for a more accurate assessment of coastal hazards. However, two of the main limitations of this study lie in the representation of grain size and seabed roughness. First, a single grain size value was used in the simulation, whereas in oceanic and coastal environments, granulometry is highly variable. The presence https://doi.org/10.5194/egusphere-2025-4986 Preprint. Discussion started: 14 November 2025





EGUsphere Preprint repository

of sediments with different sizes and properties can significantly influence tsunami behavior, as well as erosion, transport, and deposition processes. Second, seabed roughness was kept constant, even though it varies spatially in real scenarios, which can also affect wave propagation and inundation dynamics. Therefore, future research should incorporate a more representative grain size distribution and variable roughness, which will improve the accuracy of sedimentary impact estimations and optimize coastal risk mitigation strategies. Additionally, it is crucial to account for varying tide levels or conduct simulations with dynamic tides, as these factors can significantly impact inundation dynamics and sediment transport, particularly due to sea-level fluctuations. Furthermore, modeling should include post-tsunami morphological recovery or coastal dynamics, as coastline modification caused by sediment transport can generate long-term effects that must be assessed.

Supplementary: Worst-case scenario for the Colombian-Ecuadorian subduction zone

See table in supplementary files

Author contributions. R.E.S.E., J.J.F: Writing – review & editing, Writing – original draft, Visualization, Validation, Supervision, Software, Methodology, Investigation, Funding acquisition, Formal analysis, Data curation, Conceptualization. E.R.V-R., E.M.: Writing – review & editing, Supervision, Methodology, Investigation, Conceptualization

Competing interests. The authors declare no conflict of interest.

Acknowledgements. The authors would like to thank the Dirección General Marítima – Centro de Investigaciones Oceanográficas e Hidrográficas del Pacífico (DIMAR–CCCP) for providing data, information, and computational support, which were essential for the development of this study. We acknowledge the Universidad del Norte - GEO4 Geosciences Research Group for their advice, and the Co-Creation Center at the International Research Institute of Disaster Science, as well as the Core Research Cluster of Disaster Science at Tohoku University (a Designated National University), for their support.





#### References

290

295

300

- Adriano, B., Jimenez, C., Mas, E., and Koshimura, S.: Revising the seismic source of the 1979 Tumaco–Colombia earthquake (Mw 8.1) for future tsunami hazard assessment, Physics of the Earth and Planetary Interiors, 362, 107 344, https://doi.org/10.1016/j.pepi.2025.107344, 2025.
  - Apotsos, A., Gelfenbaum, G., and Jaffe, B.: Process-based modeling of tsunami inundation and sediment transport, Journal of Geophysical Research: Earth Surface, 116, https://doi.org/10.1029/2010JF001797, 2011.
- Caballero, L. and Ortiz, M.: Evaluación del impacto de tsunamis en el litoral Pacífico colombiano, Boletín Científico CCCP, pp. 45–37, 2003.
  Cantero, Y. C., Astaiza, C. A., Mesías, A. M., and Quintero, P. A.: Estudio de la tasa de sedimentación y erosión en el sector La Barra del canal navegable en San Andrés de Tumaco, Nariño, Boletín Científico CIOH, 42, 7–25, https://doi.org/10.26640/22159045.2023.611,
  - Cardona, Y., Toro, F., Vélez, J., and Otero, L.: Pacific coast tsunami modeling, Colombian: Bahía de Tumaco case, Avances en Recursos Hidraulicos, 12, 43–54, 2005.
  - Cheng, W. and Weiss, R.: On sediment extent and runup of tsunami waves, Earth and Planetary Science Letters, 362, 305–309, https://doi.org/10.1016/j.epsl.2012.12.004, 2013.
  - Collot, J.-Y., Michaud, F., Alvarado, A., Marcaillou, B., Sosson, M., Ratzov, G., Migeon, S., Calahorrano, A., and Pazmiño, A.: Visión general de la morfología submarina del margen convergente de Ecuador–Sur de Colombia: implicaciones sobre la transferencia de masa y la edad de la subducción de la Cordillera de Carnegie, Tech. Rep. PSE001-09, CNDM–INOCAR–IRD, Guayaquil, Ecuador, 2009.
  - DANE: Resultados y proyecciones (2020–2035) del censo 2018, Tech. rep., Departamento Administrativo Nacional de Estadistica, accessed 13 March 2024, 2018.
  - Deltares: Delft3D Flow User Manual, available at: https://content.oss.deltares.nl/delft3d4/Delft3D\_FLOW\_User\_Manual.pdf, 2023.
  - Guerrero, A. and Sánchez, R.: Construcción base de datos de escenarios de tsunami para el Pacífico colombiano, Tech. rep., Centro de Investigaciones Oceanográficas e Hidrográficas (CIOH), https://doi.org/10.26640/22159045.425, 2016.
  - Gutscher, M. A., Malavieille, J., Lallemand, S., and Collot, J.-Y.: Tectonic segmentation of the North Andean margin: Impact of the Carnegie Ridge collision, Earth and Planetary Science Letters, 168, 255–270, 1999.
  - Jaffe, B., Goto, K., Sugawara, D., Gelfenbaum, G., and Selle, S.: Uncertainty in tsunami sediment transport modeling, Journal of Disaster Research, 11, 647–661, 2016.
- Lesser, G., Roelvink, J., van Kester, J. A. T. M., and Stelling, G.: Development and validation of a three-dimensional morphological model, Coastal Engineering, 51, 883–915, 2004.
  - Linlin, L. and Zhenzhua, H.: Modeling the change of beach profile under tsunami waves: A comparison of selected sediment transport models, Journal of Earthquake and Tsunami, 7, 2013.
- Mas, E., Koshimura, S., Imamura, F., Suppasri, A., Muhari, A., and Adriano, B.: Recent Advances in Agent-Based Tsunami

  Evacuation Simulations: Case Studies in Indonesia, Thailand, Japan and Peru, Pure and Applied Geophysics, 172, 3409–3424, 
  https://doi.org/10.1007/s00024-015-1105-y, 2015.
  - Mas, E., Moya, L., Gonzales, E., and Koshimura, S.: Reinforcement learning-based Tsunami evacuation guidance system, International Journal of Disaster Risk Reduction, p. 105023, https://doi.org/10.1016/j.ijdrr.2024.105023, 2024.



330



- Masaya, R., Suppasri, A., Yamashita, K., Imamura, F., Gouramanis, C., and Leelawat, N.: Investigating beach erosion related with tsunami sediment transport at Phra Thong Island, Thailand, caused by the 2004 Indian Ocean tsunami, Natural Hazards and Earth System Sciences, 20, 2823–2841, https://doi.org/10.5194/nhess-20-2823-2020, 2020.
  - Ning, D., Wang, R., Chen, L., Li, J., Zang, J., Cheng, L., and Liu, S.: Extreme wave run-up and pressure on a vertical seawall, Applied Ocean Research, 67, https://doi.org/10.1016/j.apor.2017.07.015, 2017.
- Okada, Y.: Internal deformation due to shear and tensile faults in a half-space, Bulletin of the Seismological Society of America, 82, 1018–320 1040, 1992.
  - Otero, L. and González, E.: Regeneración de la Isla Barrera el Guano como un elemento protector de Tumaco frente a la acción de tsunamis: evaluación preliminar, in: Proceedings of the XXI Congreso Latinoamericano de Hidáulica, IAHR, pp. 283–294, São Pedro, Brazil, 2004.
  - Poveda, E. and Pulido, N.: Earthquake rupture and slip scenarios for the Ecuador–Colombia subduction zone, Tech. rep., Servicio Geológico Colombiano (SGC), Bogotá, Colombia, available at: http://sismo.sgc.gov.co:90/, 2019.
- Rivas, M.: Evaluación de la vulnerabilidad de las viviendas de madera en San Andrés de Tumaco ante cargas de sismo y tsunami, Tech. rep., Universidad Nacional de Colombia, 2020.
  - Sánchez, R. and Puentes, M.: Estimation of the tsunami threat in the municipality of San Andrés de Tumaco, Colombian Pacific, using LiDAR information, Boletín Científico CIOH, 30, 29–42, https://doi.org/10.26640/22159045.241, 2012.
  - Sánchez, R., Otero, L., and De la Rosa, R.: Modelado numérico de tsunamis: caso de estudio, in: Estudio de la amenaza por tsunami y gestión del riesgo en el litoral Pacífico colombiano, chap. III, DIMAR, 2013.
  - Sánchez, R., Otero, L., Guerrero, A. M., Galindo, M. P., Mas, E., Koshimura, S., and Quintero, P.: Tsunami hazard assessment for the central and southern Pacific coast of Colombia, Coastal Engineering Journal, 62, 540–552, https://doi.org/10.1080/21664250.2020.1818362, 2020
- Shimozono, T., Sato, S., and Tajima, Y.: Numerical study of tsunami run up over erodible sand dunes, in: Coastal Sediments 2011, https://doi.org/10.1061/40926(239)84, 2012.
  - Stelling, G. S. and van Kester, J. A. T. M.: On the approximation of horizontal gradients in sigma coordinates for bathymetry with steep bottom slopes, International Journal for Numerical Methods in Fluids, 18, 915–955, 1994.
  - Sugawara, D., Goto, K., and Jaffe, B. E.: Numerical models of tsunami sediment transport: Current understanding and future directions, Marine Geology, 352, 295–320, https://doi.org/10.1016/j.margeo.2014.02.002, 2014.
- Takahashi, T., Kurokawa, T., Fujita, M., and Shimada, H.: Hydraulic experiment on sediment transport due to tsunamis with various sand grain size, Journal of Japan Society of Civil Engineers, Ser. B2 (Coastal Engineering), 67, I\_231–I\_235, 2011.
  - Universidad del Norte and DIMAR: Informe de evaluación de impacto por tsunami y efectividad de obras o alternativas blandas y fuertes de mitigación seleccionadas. Proyecto: estudios para implementación de acciones para mitigar los efectos por amenaza de tsunami y cambio climático en los municipios de Tumaco y Francisco Pizarro, unpublished report, 2021.
- Usselmann, P.: Geodinámica y ocupación humana del litoral pacífico en el sur de Colombia y en el Ecuador desde el Holoceno (ultimos 10 000 años), Bulletin de l'Institut français d'études andines, 39, 589–602, 2010.
  - van Rijn, L. C.: Unified view of sediment transport by currents and waves. II: Suspended transport, Journal of Hydraulic Engineering, 133, 668–689, 2007.
- Velasco-Reyes, E. R., Sugawara, D., and Adriano, B.: Tracing the sources of paleotsunamis using Bayesian frameworks, Communications

  Earth & Environment, 5, 478, https://doi.org/10.1038/s43247-024-01643-w, 2024.



355



Watanabe, M., Goto, K., Bricker, J. D., and Imamura, F.: Are inundation limit and maximum extent of sand useful for differentiating tsunamis and storms? An example from sediment transport simulations on the Sendai Plain, Japan, Sedimentary Geology, 364, 204–216, https://doi.org/10.1016/j.sedgeo.2017.12.026, 2018.

Xiao, H., Young, Y., and Prévost, J.: Hydro- and morpho-dynamic modeling of breaking solitary waves over a fine sand beach. Part II: Numerical simulation, Marine Geology, https://doi.org/10.1016/j.margeo.2009.12.008, 2010.

Yamashita, K., Sugawara, D., Takahashi, T., and Imamura, F.: Numerical simulations of large-scale sediment transport caused by the 2011 Tohoku earthquake tsunami in Hirota Bay, southern Sanriku coast, Coastal Engineering Journal, https://doi.org/10.1142/S0578563416400155, 2016.